Biophysical Journal, Volume *113*

Supplemental Information

Spatially Organized β-Cell Subpopulations Control Electrical Dynamics across Islets of Langerhans

Matthew J. Westacott, Nurin W.F. Ludin, and Richard K.P. Benninger

Figure S1. Quantification of ChR2-YFP Expression in Disassociated Islets

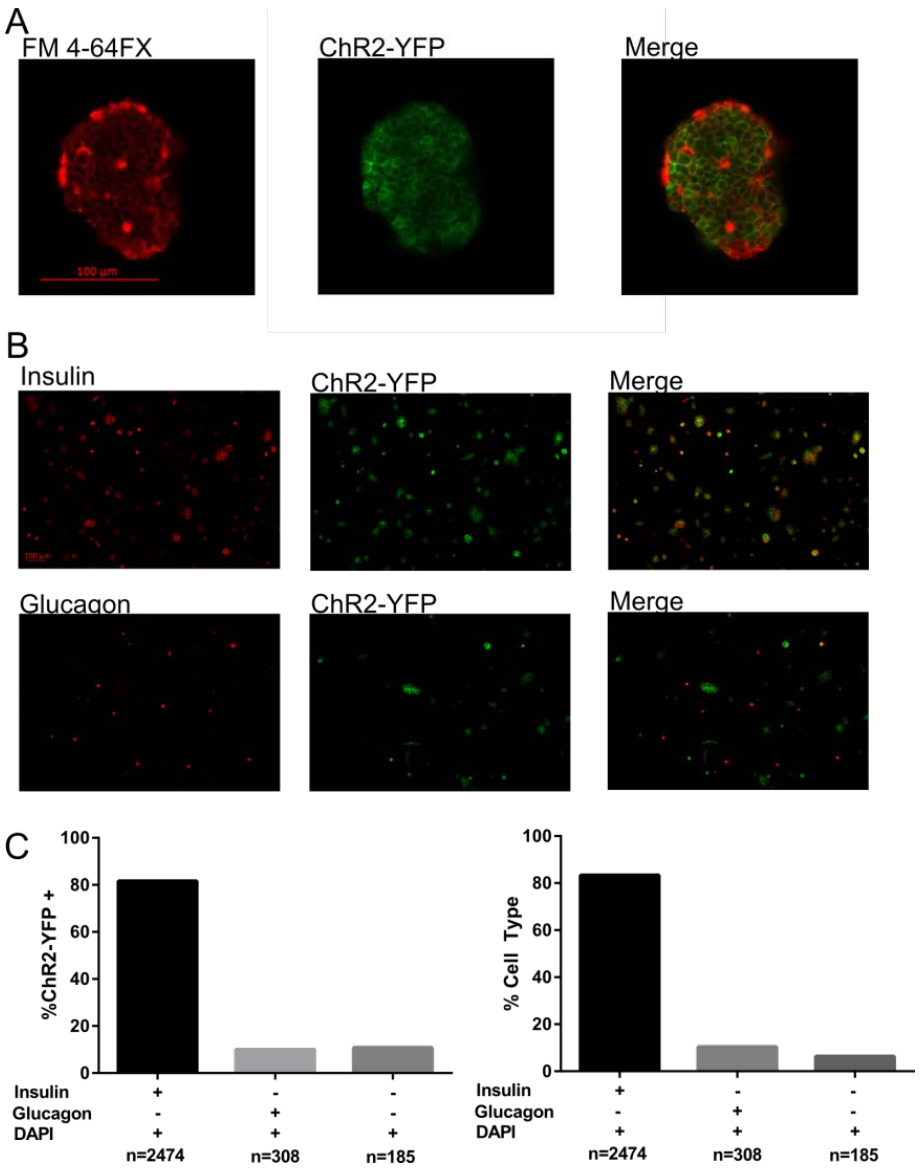

(A) Image within intact islet of plasma membrane labelled with FM 4-64FX (left); image within intact islet of ChR2-YFP distribution (middle); together with merged image (right). Expression of ChR2-YFP is high throughout the islet. (B) Representative immunofluorescence images of insulin (top, left), YFP (top, middle), and merged image (top, right); or representative immunofluorescence images of glucagon (bottom, left), YFP (bottom, middle), and merged image (bottom, right), all in dissociated cells from the islet. (C) Quantification of percentage insulin positive cells, glucagon positive cells or insulin and glucagon negative cells that express ChR2-YFP (left); and quantification of all cells (dapi positive) that are insulin positive, glucagon positive or are insulin and glucagon negative (right).

Figure S2. ChR2 activated area and NAD(P)H response have no temporal/spatial biasing

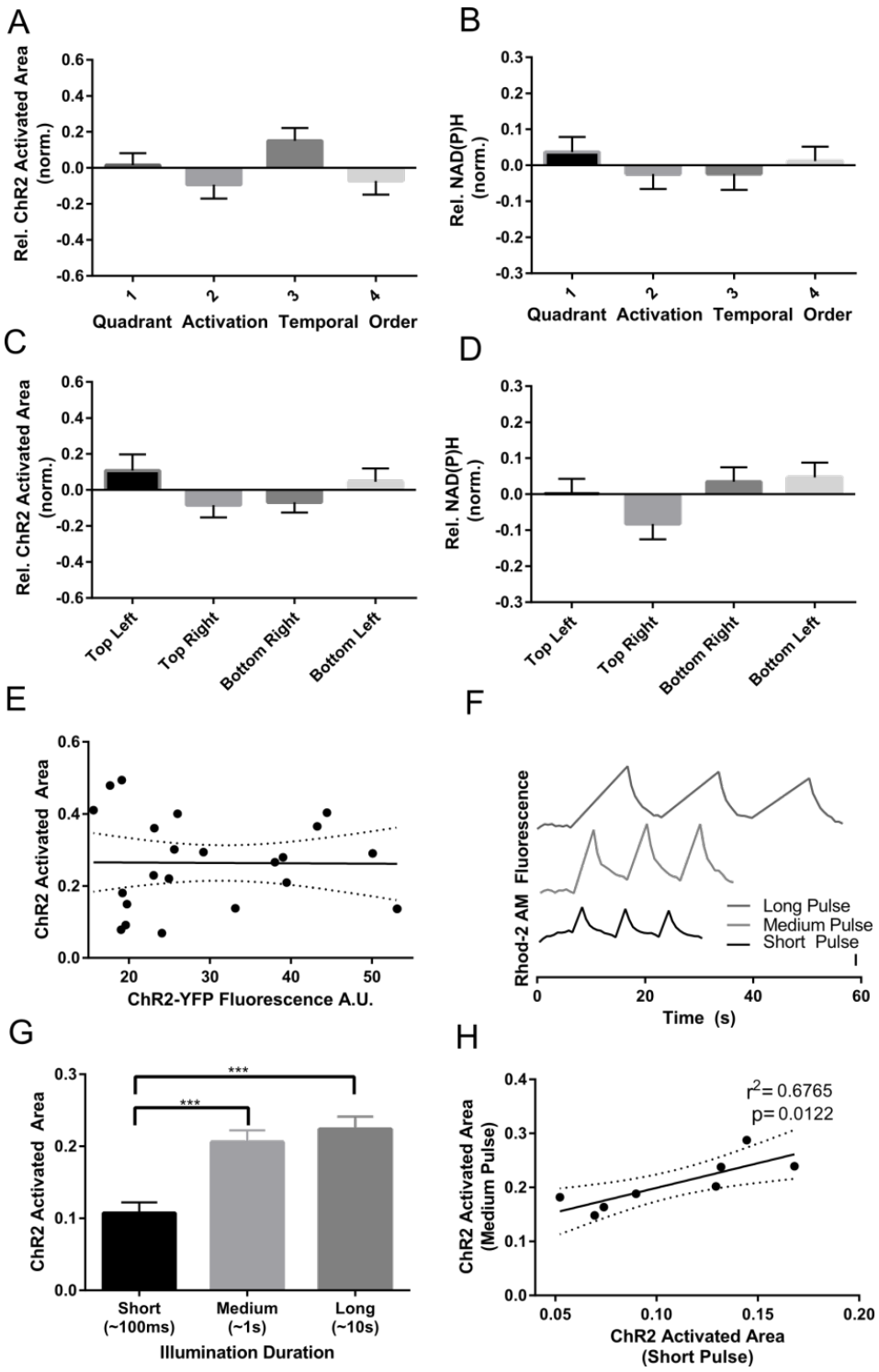

(A) Mean (±s.e.m.) ChR2 activated area relative to the islet average sorted according to the temporal order of ChR2 quadrant activation. (B) Mean (±s.e.m.) NAD(P)H response relative to the islet average sorted according to the temporal order of ChR2 quadrant activation. (C) Mean (±s.e.m.) ChR2 activated area relative to the islet average binned according to the spatial position in the field of view of ChR2 quadrant activation. (D) Mean (±s.e.m.) NAD(P)H response relative to the islet average binned according to the spatial position in the field of view of ChR2 quadrant activation. (E) Scatterplot and linear regression (+/-95% confidence intervals) for the ChR2 activated area within an islet against the YFP fluorescence averaged across the region of activation. (F)

Representative time-courses of $[Ca^{2+}]_i$ with different durations of ChR2 activation (long=10s, medium=1s, short=100ms). (G) Quantification of ChR2 activated area as a function of ChR2 activation duration. (H) Scatterplot of ChR2 activated area in quadrants with medium pulse illumination times (~1s) vs short illumination times (~100ms). Data in A-D averaged over n=25 islets, data in E, n=27 quadrants and G,H, n=8 quadrants.

Figure S3. NAD(P)H vs. ChR2-activated $[Ca^{2+}]_i$

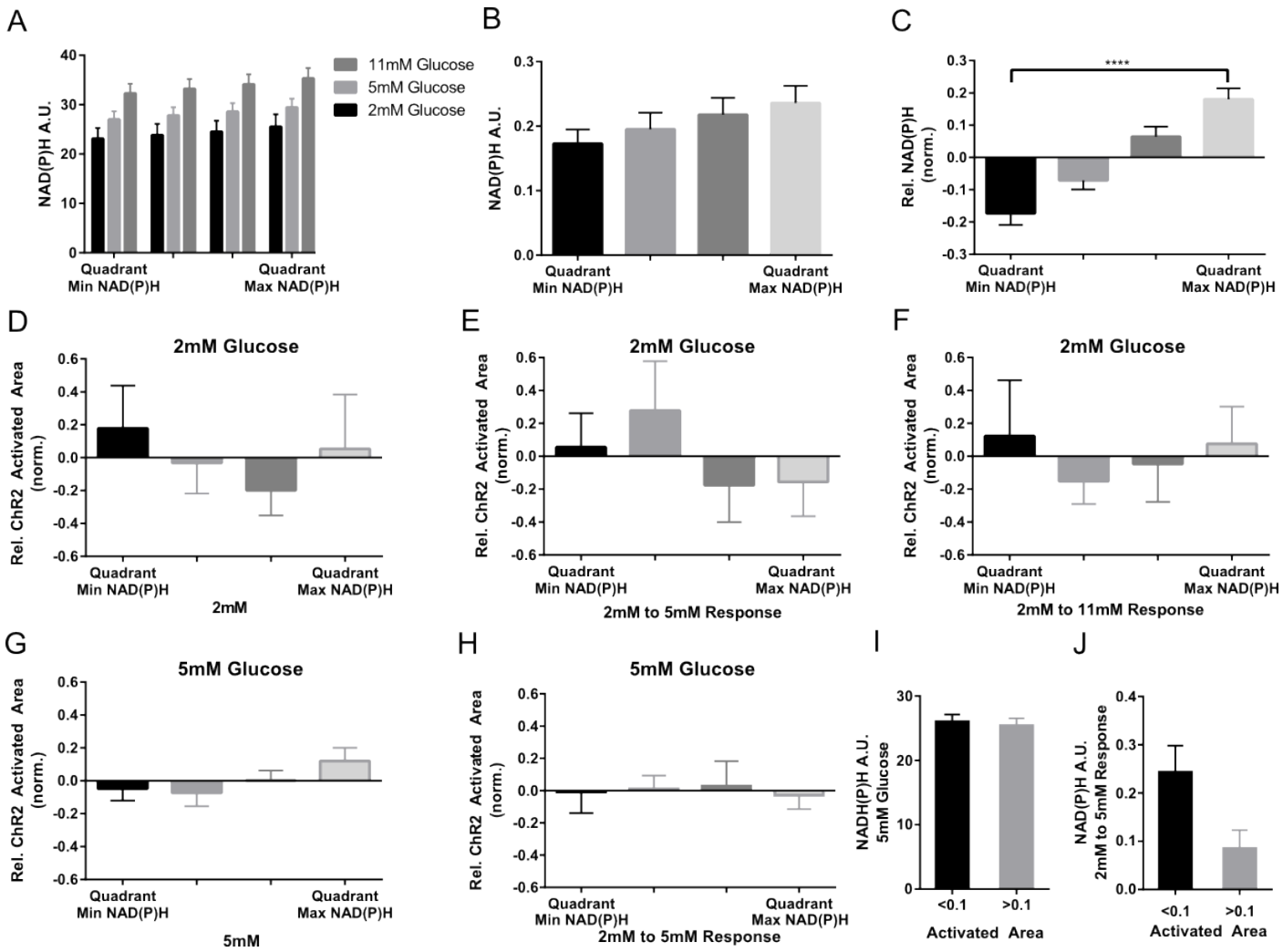

(A) Mean (±s.e.m.) NAD(P)H levels at 2mM, 5mM, 11mM glucose by quadrants, sported in ascending rank order. (B) Mean (±s.e.m) NAD(P)H response between 5 and 11mM glucose, in quadrant regions of the islet defined by ChR2 activation regions, sorted in rank order. (C) Mean (±s.e.m) intra-islet variation in NAD(P)H response relative to the islet average. The NAD(P)H response over each quadrant (as in B) was expressed relative to the mean NAD(P)H response over the whole islet, and sorted from least to most. (D) Mean (±s.e.m) ChR2 activated area relative to the islet average resulting from quadrant regions of activation at 2mM glucose, for each corresponding rank-ordered NAD(P)H level over the region at 2mM glucose. (E) Mean (±s.e.m) ChR2 activated area relative to the islet average resulting from quadrant regions of activation at 2mM glucose, for each corresponding rank-ordered NAD(P)H response over the region between 2mM and 5mM glucose. (F) As in D for ChR2 activated area at 2mM glucose, for corresponding NAD(P)H response between 2mM and 11mM glucose. (G) As in D for ChR2 activated area at 5mM glucose, for corresponding NAD(P)H level at 5mM glucose. (H) As in D for ChR2 activated area at 5mM glucose, for corresponding NAD(P)H response between 2mM and 5mM glucose. (I) Mean (±s.e.m) NAD(P)H level at 5mM glucose for single cell activation regions in which ChR2 activated area was low (<0.1), high (>0.1). (J) As in H for NAD(P)H response between 2mM and 5mM glucose. Data in **a**-**c** averaged over n=25 islets from 6 mice; data in **d**-**h** averaged over n=10 islets from 3 mice; data in **i**,**j** averaged over n=96 regions, 26 islets from 5 mice. **** indicates p<0.0001 comparing

experimental groups indicated. A Benjamini–Hochberg procedure and Bonferroni correction was applied to data in D-H (with data in Figure 2 B). Students T-Test was used in I,J to calculate statistical significance.

Figure S4. Cx36 gap junction permeability vs. ChR2-activated $[Ca^{2+}]_i$.

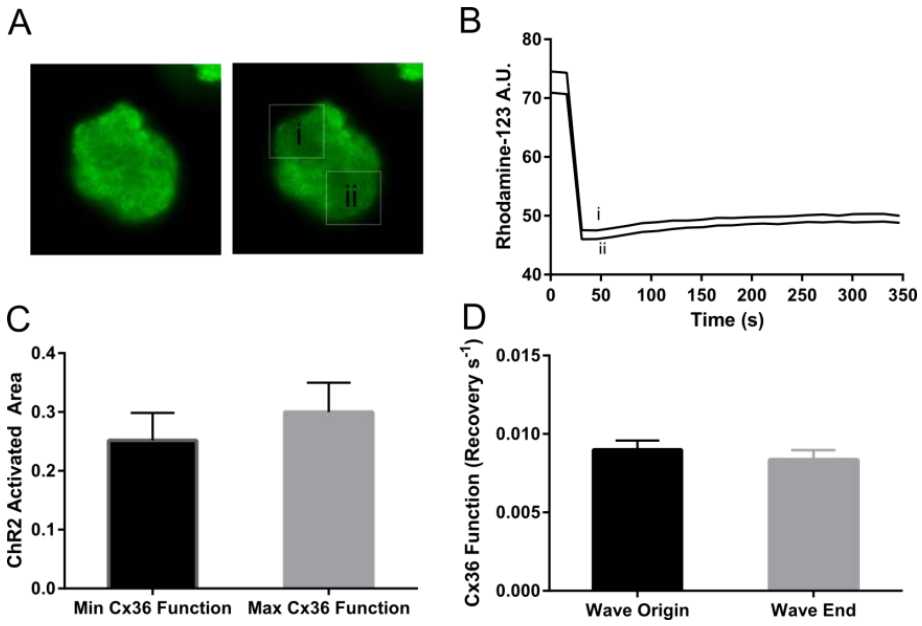

(A) Left: Representative islet with showing Rhodamine-123 fluorescence prior to photobleaching (left) and post photobleaching in the two indicated quadrants (right). (B) Time-course of Rhodamine-123 fluorescence from islet in (A), before, during and after photobleaching. (C) Mean (±s.e.m.) ChR2 activated area for quadrant of islet showing minimal and maximal Cx36 permeability. (D) Mean (±s.e.m.) Cx36 permeability (recovery rate) for quadrants of wave origin and wave end. Data in C-D averaged over n=16 and n=12 islets respectively. Students T-test used to test for significance in C-D.

Figure S5. Heterogeneity in ChR2-activated membrane depolarization in simulated islet.

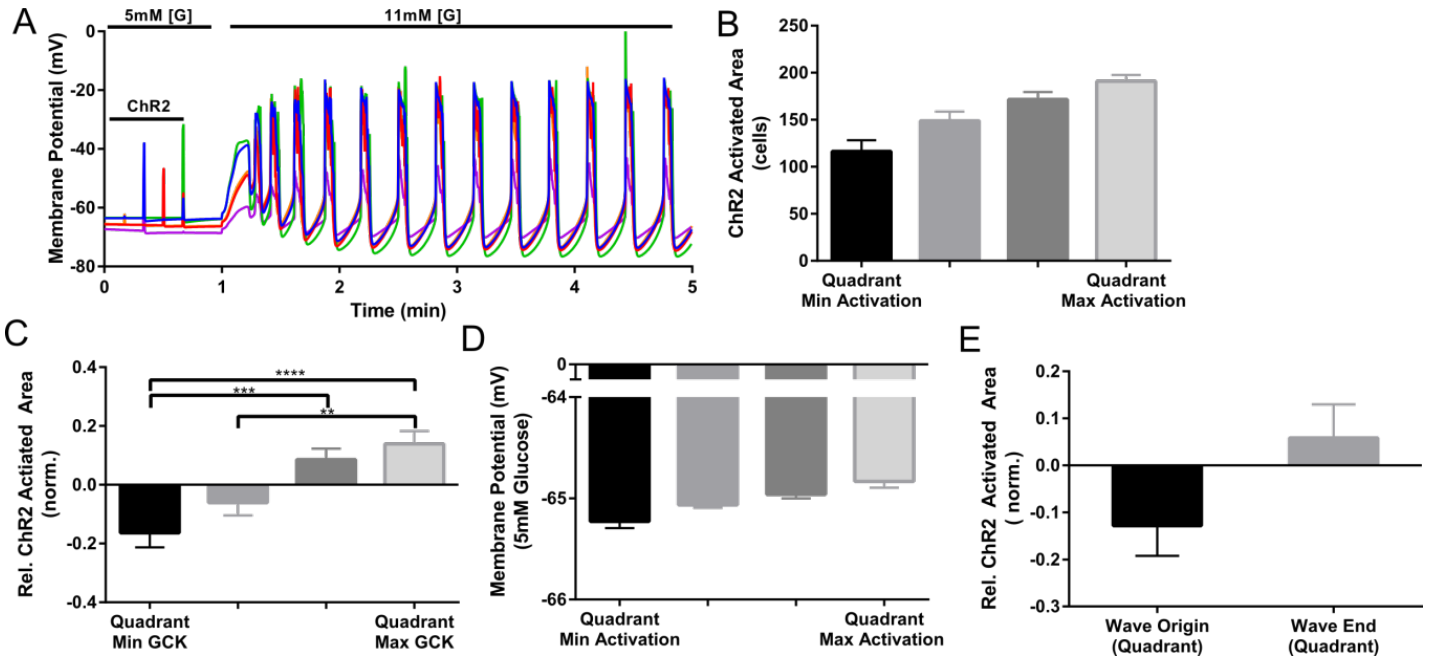

(A) Representative time courses of membrane potential from 4 cells within a simulated islet with spatially ordered metabolic activity (as in Figure 4). (B) Mean (±s.e.m.) ChR2 activated area of membrane depolarization from **a**, for each quadrant of the islet in ascending rank order. Vm=-40mV was used as a cutoff between active and inactive cell during ChR2 activation. (C) Mean (±s.e.m.) ChR2 activated area relative to the islet average, for each quadrant of ascending GCK rate (metabolic activity). (D) Mean (±s.e.m.) resting membrane potential at 5mM glucose, for each corresponding ascending rank-order quadrant of ChR2 activated area. Data in B-E average over n=30 simulated islets. (E) Mean (±s.e.m) ChR2 activated area relative to the islet average in quadrants of wave origin and wave end.

Figure S6. Spatial domains to K_{ATP} channel density partially recapitulate experimental ChR2-activated $[Ca^{2+}]_i$ and calcium wave measurements.

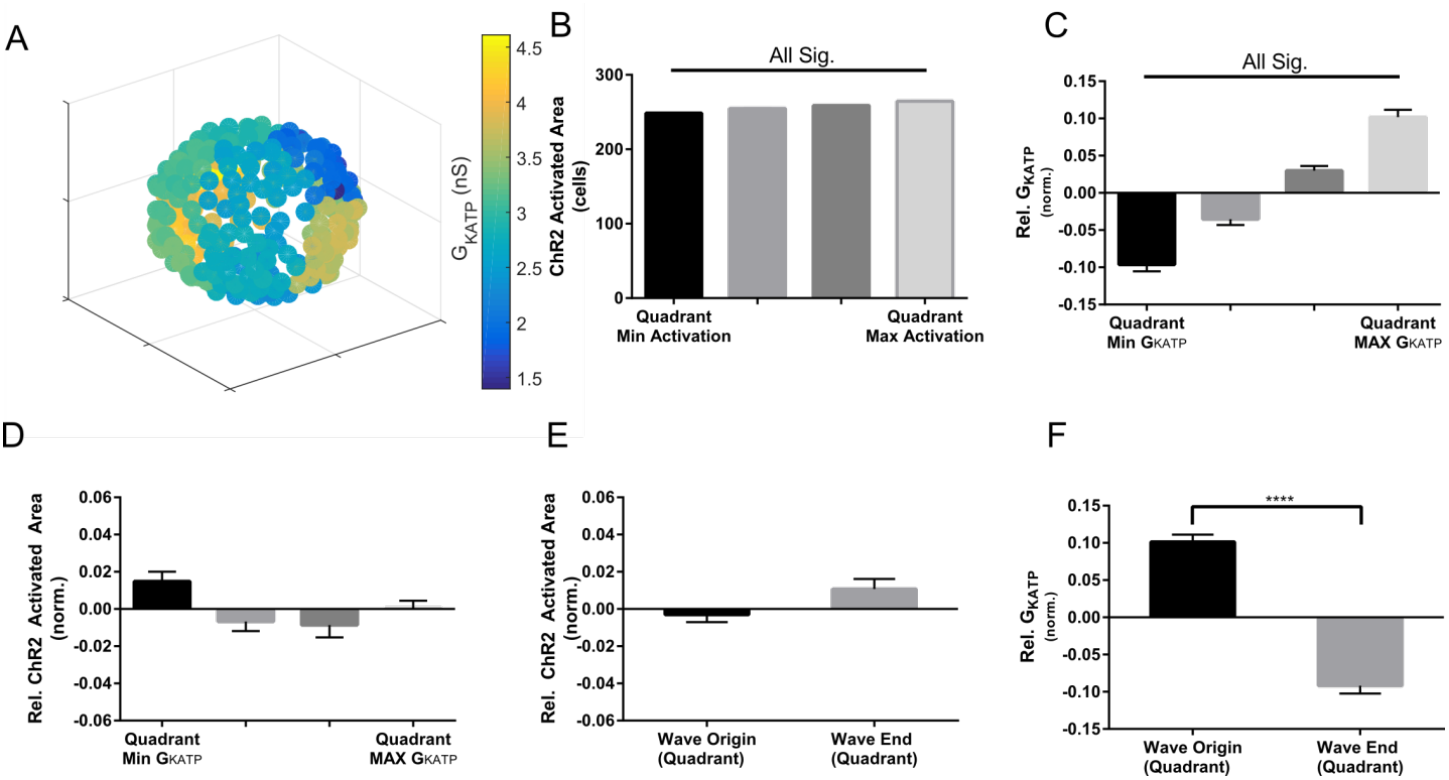

(A) Representative false-color map showing cellular K_{ATP} channel conductance (G_{KATP}) over a simulated islet, where subregions of similar heterogeneity is applied. Each circle represents a simulated β-cell. (B) Mean (±s.e.m.) ChR2 activated area (cells) by quadrants in ascending rank order. (C) Mean (±s.e.m) intra-islet variation in G_{KATP} relative to the islet average. The G_{KATP} over each quadrant was expressed relative to the mean G_{KATP} over the whole islet, and sorted from least to most. (D) Mean (±s.e.m) ChR2 activated $[Ca^{2+}]_i$ relative to the simulated islet average, for each corresponding ascending rank-ordered quadrant G_{KATP} (as in B). (E) Mean (±s.e.m.) area of ChR2 activated $[Ca^{2+}]_i$ relative to the islet average, in quadrant of wave origin and wave end. (F) Mean (±s.e.m.) G_{KATP} relative to the islet average, in quadrats of wave origin and wave end from E. Data in C-F averaged over n=25 simulated islets. **** indicates $p<0.0001$ comparing experimental groups indicated. Students T-Test was used in E,F to calculate statistical significance.

Figure S7. Spatial analysis of ChR2-activated [Ca^{2+}] responses.

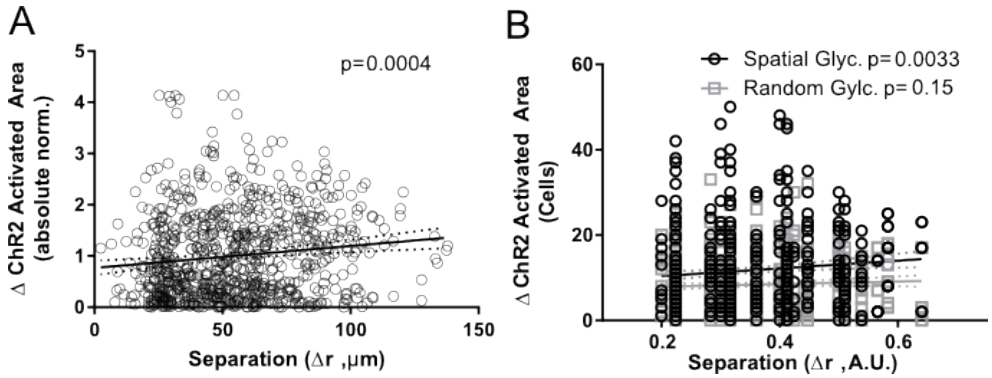

(A) Pairwise absolute differences in ChR2 activated [Ca^{2+}] area between cells as a function of spatial separation, together with linear regression from Fig 4G,H. (B) Equivalent analysis as **A,** done in simulated islets with either spatial dependent GK distribution (black circles) or random spatial GK distribution (grey squares), from Fig 4I. Regression lines fit using linear least squares method and significance in slope determined using F-test.

Table S1. Parameters used for islet model. Heterogeneity is based on a Gaussian distribution, unless otherwise indicated, with a standard deviation as a percentage of the mean value (σ=%μ).

Independent Variable	Description	Value
C_m	Cell Capacitance	6.158pF
vol_i	Cytosolic Volume	764fl
vol_{er}	Endoplasmic Reticulum Volume	280fl
f_i	Cytosolic Ca^{2+} Buffer Strength	0.01
f_{er}	ER Ca^{2+} Buffer Strength	0.025
P_{CaV}	Converting factor for I_{CaV}	48.9 pA mM^{-1}
P_{KDr}	Converting factor for I_{KDr}	2.1 pA mM^{-1}
$G_{KCA(BK)}$	Conductance of $I_{KCa(SK)}$	2.13 pA mV^{-1}(10%)
$P_{KCA(SK)}$	Converting factor of $I_{KCa(SK)}$	0.2 pA mM^{-1}
P_{bNSC}	Converting factor of I_{bNSC}	0.00396 pA mM^{-1}
P_{SOC}	Converting factor of I_{SOC}	0.00764 pA mM^{-1}
$K_{0.5ER}$	Half activation conc. Of Ca^{2+} in ER	0.003 mM
$G_{K(ATP)}$	Max conductance of I_{KATP}	2.57 pA mV^{-1}(25%)
G_{coup}	Average conductance of Cx36	0.12 pS (40%)
P_{NaK}	Max amplitude of I_{NaK}	350 Pa ms
P_{NaCa}	Max amplitude of I_{NaCa}	204 pA (10%)
P_{PMCA}	Max amplitude of I_{PMCA}	1.56 pA
P_{SERCA}	Max pump rate of Ca^{2+} into ER	0.065 fl ms^{-1} (10%)
P_{Rel}	Converting factor for ER Ca^{2+} release	0.76 fl ms^{-1} (10%)
k_{glc}	Rate constant for glycolysis	0.000076 (25%)
$K_{\beta ox}$	Rate constant of β-oxidation	0.0000063 ms^{-1} (10%)
Po_p	Max rate of ATP production	0.0005 ms^{-1} (10%)
$[ATP_{tot}]$	Total ATP species	4mM(10%)
k_{ATP}	Rate Const. of Ca^{2+} ind. Ca^{2+} consumption	0.00062 ms^{-1}
$k_{ATP,Ca}$	Rate Const. of Ca^{2+} dep. ATP consumption	0.187 mM^{-1} ms^{-1}
$k_{ADP,f}$	Rate Const. of ADPf to ADPb	0.0002 ms^{-1}
$k_{ADP,b}$	Rate Const. of ADPb to ADPf	0.00002 ms^{-1}

Movie S1 ChR2 Activation in the islet model: Representative simulation of $[Ca^{2+}]_i$ activity while activating each quadrant with ChR2 current source. Glucose is held at 5mM in parallel with *ex-vivo* experiments.

Movie S2 Wave dynamics in islet model: Glucose is stepped up between 5mM and 11mM inducing initial $[Ca^{2+}]_i$ influx before settling in to persistent $[Ca^{2+}]_i$ oscillations.

Movie S3 Representative $[Ca^{2+}]$ oscillations in $Cx36^{-/-}$ islet at 11mM glucose.